Analyst

PAPER

View Article Online
View Journal | View Issue

Cite this: *Analyst*, 2024, **149**, 2338

Time and spatially resolved VIS-NIR hyperspectral imaging as a novel monitoring tool for laser-based spectroscopy to mitigate radiation damage on paintings†

Amelia Suzuki, [a,b] C. S. Cheung, [a] Yu Li, [a] Alexander Hogg, [a] Patrick S. Atkinson,[a] Cristiano Riminesi, [b] Costanza Miliani[c] and Haida Liang *[a]

The increased adoption of non-invasive laser-based techniques for analysis of cultural assets has recently called into question the non-invasiveness of the techniques in practical operation. The methods to assess the occurrence of radiation-induced alteration on paintings are very limited and none of them can predict damage. Here we present a novel multimodal imaging approach to understand the time and spatial evolution and types of laser-induced surface alterations, through simultaneous monitoring using visible and near infrared (VIS-NIR) reflectance hyperspectral imaging (HSI) and thermal imaging during Raman spectroscopy. The resultant physical and chemical changes were examined in detail by optical coherence tomography and synchrotron based micro-X-ray powder diffraction. HSI was found to be the most sensitive in detecting laser induced alternations compared with conventional methods. It is orders of magnitude more sensitive than Raman spectroscopy and even synchrotron-based micro-X-ray powder diffraction. In cases of thermally driven alterations, transient and reversible reflectance changes were found to be the first indications of laser-induced modifications and can therefore be used as precursors to prevent damage. VIS-NIR reflectance spectroscopy should be used to monitor laser-based analysis and potentially other radiation-based techniques *in situ* to mitigate laser induced alteration.

Received 24th November 2023,
Accepted 29th January 2024

DOI: 10.1039/d3an02041j

rsc.li/analyst

1. Introduction

The advancement in mobile 'non-invasive' analytical techniques has been a major technological contribution to the adoption of scientific analysis in the characterization of artists' materials and their possible degradation products, owing to the ease of application to historical cultural assets *in situ*.[1] Mobile instruments sometimes make use of intense radiation such as lasers. Despite it is known that intense radiations (lasers and ionizing radiations) can increase the probability of damage on cultural heritage materials,[2] research effort is still needed to better understand the radiation-matter interaction, identify the critical parameters and develop monitoring methods to better design strategies to reduce the risk associated with the use of intense radiations. The importance of the problem is demonstrated by its inclusion in one of the scientific objectives of a pan-European project.[3] Any alteration of artworks must be minimized as much as possible as the integrity of culturally significant artworks is a strict requirement governed by conservation ethics. The samples collected from artworks also need to be preserved to guarantee future analysis, as they represent invaluable resources of information for scientists, conservators, archaeologists, art historians and curators.

Within laser-based techniques, Raman spectroscopy is one of the most well-established techniques thanks to its high specificity for molecular characterization[4] especially used for pigment analysis.[5] Its increased use in recent years has challenged conventional assumption of non-invasiveness, especially for the development of macro-Raman mapping which can affect a significant area of the artwork.[6,7] When dealing with pigments, some damage may occur upon laser irradiation,[5,8,9] and if laser-induced transformation occurs, the reliability of the data acquired and the materials identified can be questioned.[10]

Laser-induced damage denotes any permanent change in the characteristics of the surface or bulk of a specimen that

[a]*Imaging and Sensing for Archaeology, Art History and Conservation (ISAAC) Lab, School of Science and Technology, Nottingham Trent University, Nottingham NG11 8NS, UK. E-mail: haida.liang@ntu.ac.uk*
[b]*Institute of Heritage Science – National Research Council, ISPC-CNR, Via Madonna del Piano 10, Sesto Fiorentino (FI), 50019, Italy*
[c]*Institute of Heritage Science – National Research Council, ISPC-CNR, Via Cardinale Guglielmo Sanfelice, 8, 80134 Napoli, Italy*

†Electronic supplementary information (ESI) available: Fig. S1 to S9. See DOI: https://doi.org/10.1039/d3an02041j

can be observed by an inspection technique[11] and is a function of material properties, laser parameters and to some extent environmental conditions (*e.g.*, humidity and temperature). Visual observation or assessment under optical microscopes are the most frequent inspection techniques adopted, even though some damages are difficult to see in plain sight.[2,12] When performing Raman spectroscopy, a common monitoring strategy consists of detecting changes in the Raman spectra itself, such as peak broadening, shifting,[9,13] a decrease of the peak intensities,[14] or new peaks emerging due to phase transformation.[8] These particular changes in Raman spectra have been analysed in detail to understand if they can be taken as indicators for the detection of damage. Based on these Raman changes, the laser-induced damage threshold (LIDT) expressed in intensity (power per unit area), has been defined for a few pigment powders, such as lead-based pigments (red lead, lead white, litharge, massicot and plattnerite),[8] Prussian blue[9] and vermilion.[14] The use of Raman spectral changes for the detection of damage is convenient as it is integrated in the measurement itself. However, this monitoring often fails in the detection of damage, *e.g.*, no Raman spectral changes were detected despite discoloration observed in phthalocyanine,[13] indigo[15] or chrome yellow.[16] Our recent studies found that the two commonly employed inspection techniques, visual observation and Raman monitoring, are also not sensitive enough to detect some short-term alterations on paints that can be detected only with visible and near infrared (VIS-NIR) reflectance spectroscopy.[6,17,18] Although visual inspection and Raman spectroscopy can offer useful guidance for the detection of certain laser-induced damages, they can be blind to physical changes (*e.g.*, partial melting of the surface) and inter and intra molecular scale damage below the detection limit. In some cases, the alteration may not correspond to damage of the pigment (*e.g.*, alteration in the binding medium). LIDT expressed in terms of the minimum laser intensity (power per unit area) at which a damage is observed, is usually determined on mock-ups to avoid causing damage to the real paintings by gradually increasing laser power. This method is often unrepresentative of real cases because of numerous material parameters that can vary the damage probability on real artists' materials. One example is the particle size, reported to affect the phase transformation of iron oxide nanoparticles[19] and blackening of azurite.[20] The degree of crystallinity can also modify the laser damage susceptibility of a material.[21] Another key factor is the presence of impurities as highlighted in Ciofini *et al.*,[22] where different batches of lead white heated up differently upon the same irradiation condition as a result of varying concentration of impurities of iron oxides. Therefore, the identification of LIDT on artificial samples does not represent a successful strategy to avoid radiation damage. Instead, research effort should aim at developing on-line monitoring methods to prevent damage.

A very useful monitoring method has been designed by Mencaglia *et al.*[23,24] that enables adjustment of the Raman laser power based on simultaneous thermal monitoring of the irradiated surface. However, the fundamental limitations are that thermal damage thresholds of materials are not always known *a priori*, and laser-induced alterations may not always result in a significant increase of surface temperature, *e.g.*, photochemically dominated reactions. Therefore, the development of alternative monitoring methods for comprehensive damage detection is still in demand.

In this work, we present a new multi-modal analytical approach for monitoring radiation damage due to the interaction between continuous wave (CW) lasers commonly employed in Raman spectroscopy and artists' paint materials. The set-up consists of time- and spatially resolved hyperspectral imaging (HSI) for VIS-NIR (400–900 nm) reflectance spectroscopy and IR-thermography. To verify the sensitivity to damage detection of this new method, a comparison with Raman monitoring method is performed. Optical coherence tomography (OCT) is used to confirm morphological surface changes, and synchrotron based micro-X-ray powder diffraction (SR μ-XRPD) mapping is performed to assess the possible crystal structure changes of the pigments induced by the lasers. The proof of concept of the method is demonstrated through the detection of physical and/or chemical damages while irradiating oil paint containing 3 red-orange pigments that show similar absorption and scattering properties in the visible regime but different behaviour upon laser irradiation. The data obtained by this multi-modal approach allow the distinction between thermal or non-thermal effects thanks to specific changes in spectral reflectance. Of particular interest is the possibility to objectively define safety thresholds based on transient and reversible reflectance spectral changes that are precursors to the occurrence of more permanent damage. Based on the survey of the main laser and material parameters that are relevant to the risk of damage, experimental strategies for damage prevention are discussed.

2. Experimental

2.1 Mock-up samples

Irradiation tests were performed on mock-ups designed to simulate a naturally aged oil painting on panel: 15 years old oil paint mock-ups[25] with pigments reported as unstable to laser irradiation (vermilion, realgar and red lead).[5,6,8] The selection of the oil painting mock-ups was made to assess potential damage in realistic examples representing a real painting. The studies performed up to now concerning laser-induced damage were performed on pressed pigment powders.[8,9,14] For comparison with literature, irradiation tests were also performed on vermilion pigment powder. The pigments were mixed with linseed oil and applied on a preparation layer of chalk in rabbit skin glue on a plywood substrate. The paint thickness is *ca.* 200 μm. The pigments were selected to have similar reflectance spectra: all three pigments absorb at 532 nm while they are all strong scatterers at 785 and 1064 nm. Moreover, the pigments show different light and thermal stability, which are key material parameters that influence the occurrence of radiation damage. Realgar (As_4S_4) rep-

resents one of the most light-sensitive[26] and thermally unstable pigments (up to 200 °C),[27,28] while vermilion (α-HgS) represents a relatively light-stable pigment[29] with a low thermal stability (300 °C);[30] red lead (Pb_3O_4) is considered a relatively light-stable pigment with a high thermal stability (up to 600 °C).

2.2. Multi-modal imaging set up for monitoring

The set up for the multi-modal monitoring of laser irradiation is shown in Fig. 1. The monitoring consists of recording the VIS-NIR reflectance spectra of the mock-up paint pre-irradiation (120 s) and post-irradiation (300 s). To correlate the reflectance changes with the effects of heat, a thermal imaging device was used to monitor the relative trend of the surface temperature during the experiments. Raman spectroscopy was performed to assess the spectral modification induced by the laser irradiation. The interrogating laser source is normal to the mock-up, at 3.5 m. Three different CW lasers commonly used for Raman spectroscopy were tested (532 nm fiber laser with maximum output of 100 mW, 785 nm with a maximum output of 126 mW and 1064 nm with 445 mW maximum output) at different spot sizes (from tens of μm to 900 μm), power and exposure times in order to verify the most damaging combination of parameters. All three lasers have Gaussian beams and the spot sizes on the sample were varied using different lenses. On each occasion, the spot size was measured by imaging directly onto a detector with a pixel size of 4.4 μm. The laser power on the target was measured prior to each test with a standard Thorlabs photodiode power sensor S120C with a neutral density filter of 10%. The overall range of power investigated varies between 0.015 mW and a maximum of 100 mW. As the investigated pigments are strong Raman scatterers the standard laser irradiation time was set to 10 s, which represents more than a typical integration time to collect a high signal-to-noise-ratio (SNR) Raman spectrum of these pigments. The effect of irradiation time was assessed between 10 s and 450 s. Several irradiation tests were performed on each of the mock-ups. All the tests were performed on previously un-irradiated zones of the mock-up. At first, some tests were repeated to check the homogeneity of the mock-ups and the reproducibility of the measurements (Fig. S1†), which showed a small variation in detected temperature over a range of 7% and a variation in the spectral reflectance change ΔR over a range of 0.5%.

2.2.1 VIS-NIR hyperspectral imaging. To improve the stability and spatial resolution compared to our previous study using fibre optic reflectance spectroscopy,[17] a grating-based hyperspectral imaging system was chosen which allows simultaneous monitoring of the changes within the laser spot and the surrounding area with a spatial resolution of ~15 μm at a distance of 3.2 m of an area 30 μm × 15 000 μm. The simultaneous monitoring of the surrounding area provides an internal control to evaluate the quality of each single measurement (Fig. S2†). Moreover, most thermal related damages will dissipate heat from the irradiated area, which makes it possible to evaluate the extent of the damage as a function of temperature away from the laser spot, where no photons are directly involved allowing differentiation of changes caused by heat

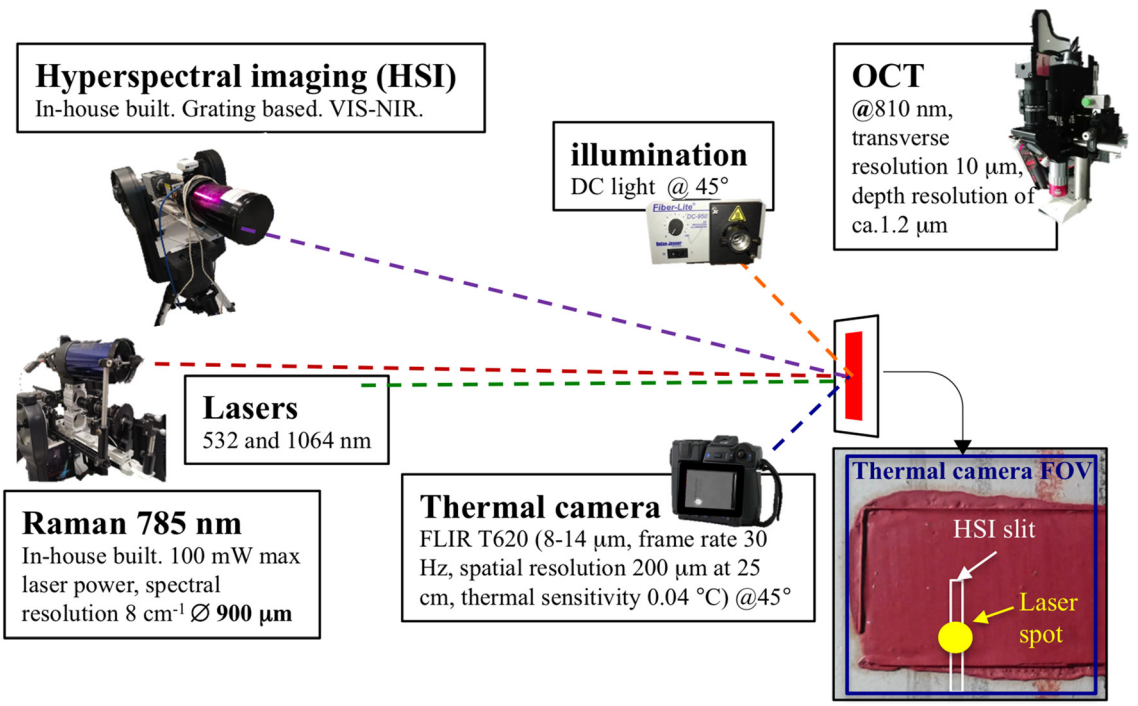

Fig. 1 The set-up for monitoring laser induced alterations and a brief description of instrument specifications. The enlarged picture of the sample shows the probing area for each technique: thermal imaging (dark blue box), hyperspectral imaging (HSI) slit (white rectangle) and the laser irradiation spot for Raman spectroscopy (yellow solid circle).

alone compared to those that involved photons. The instrument used is an in-house developed line-scan grating-based imaging system developed at the ISAAC laboratory, Nottingham Trent University, used at a distance of 3.2 m at ~60° with respect to the surface of the mock-up. The system consists of an Andor Zyla 5.2 sCMOS camera combined with a Specim ImSpector V10E spectrograph. The spectrograph provides a spectral resolution of 2.8 nm (with 30 μm slit) and after rebinning gives a total of 132 channels with spectral sampling resolution of 4.53 nm per pixel. The first few channels at the beginning and at the end were removed due to their low SNR, narrowing down the spectral range to 400–900 nm. A Meade ETX90 telescope is attached to the spectrograph and camera system. Calibration of the spectra was achieved using a 99% Spectralon© diffuse reflectance target. The reflectance spectra were recorded before (0.2 s integration time each for a total of 120 s) and after the laser irradiation (0.2 s each for a total of 300 s) at the exact same position, without scanning. For illumination, a DC light source at ~1 m and 45° to the target was used (the illumination increases the surface temperature by only 1–2 °C). The damage was evaluated based on the difference spectra between post and pre-irradiation (ΔR) plots. Internal checks on the system stability were enabled using areas along the slit of the HSI far from the position of the laser irradiation where no temperature increase is detected by the thermal camera (Fig. S2†). Any ΔR above the level of system stability and noise fluctuation were identified either as permanent or transient damage within the 300 s monitoring post irradiation.

2.2.2. Thermal imaging. The thermal camera is a FLIR T620 with a FOV of 25° × 19°, frame rate of 30 Hz and temperature range −40 °C to 650 °C. The recording was performed at 45° and at a distance of 25 cm, providing a spatial resolution of ~200 μm. Temperature was monitored for the whole duration of the experiment (before, during and after the laser irradiation) with emissivity set at 0.95 based on preliminary measurements on the specific mock-ups.

2.2.3. Raman spectroscopy. A remote standoff 785 nm Raman system developed by ISAAC lab (for details of the system refer to ref. 31) was used with a 500 l mm^{-1} grating, giving a spectral resolution of 8.5 cm^{-1}. The changes in Raman spectra were evaluated in terms of changes in net peak counts above the fluorescence continuum spectrum and peak positions. Raman spectra were recorded simultaneously while irradiating with the 785 nm laser. The same 785 nm Raman system was employed to monitor the effects of the 1064 nm and 532 nm lasers, for consistent comparison. In these cases, several Raman spectra were recorded pre and post irradiation with the 785 nm laser at 2.8 mW over 900 μm spot (the safety of this setting was previously checked with the same monitoring procedure).

2.2.4. Optical coherence tomography. For characterization of the surface and sub surface structure of the irradiated region, an in house built ultra-high resolution Fourier Domain OCT developed by ISAAC lab[32] was used, producing a 5 × 5 × 2 mm^3 virtual volume cube with depth resolution of ~2 μm in air and a transverse resolution of 10 μm. The paint surface position is extracted from the OCT cube and a root-mean-squared (RMS) surface roughness map is calculated with a 50 μm window.[33]

2.2.5. Synchrotron based micro-X-ray powder diffraction mapping. To assess the possible changes in the crystal structure of the pigments, SR-based μ-XRPD mapping was performed on thin sections of 10 μm thickness at the μ-XRD branch of ID13 beamline of the European Synchrotron Radiation Facility (ESRF, Grenoble, proposal HG172[34,35]). To perform raster scan maps, a beam size of *ca.* 2.5 × 2.5 μm^2 was used with a step size of 2 μm in x and y directions, with an acquisition time per point of 10 ms at 12.92 keV and a flux of ~1.9×10^{11} ph s^{-1} (at I = 34 mA electron beam current). The two-dimensional diffraction patterns collected in transmission have been azimuthally integrated using dedicated Jupyter notebooks, based on the PyFAI software package[36] and were then analysed with PyMCA software to perform ROI imaging.[37] The identification of the crystalline compounds was performed with Match! software using COD inorganics database.[38]

3. Results

3.1. Thermally dominant effects

Fig. 2 shows the results of the monitoring while irradiating the vermilion oil mock-up with 785 nm and 532 nm lasers at a high laser power of 100 mW. The 785 nm laser produced a spot with a milky appearance and the surface temperature reached 80 °C (Fig. 2a). The 532 nm laser, strongly absorbed by the pigment, caused a surface darkening, and reached an elevated temperature of 180 °C. The VIS-NIR percentage reflectance changes (ΔR) extracted from the hyperspectral images at a single slit position monitored over time are reported in ΔR plots by subtracting the pre irradiation spectra from the post irradiation spectra. The evolution of the ΔR plots is shown at various times immediately after the laser was turned off (from 1 to 300 s) and at different spatial offset from the center of the laser spot. A short-term ΔR change at 600 nm was detected within the first few seconds post irradiation and this corresponds to a temporary shift towards longer wavelengths at the point of inflection in the typical "S-shaped" reflectance spectrum of semiconductors. The short-term reversion of ΔR at the same wavelength was also detected outside the laser spot and gradually disappeared further out from the laser spot as the surface temperature decreased. The same ΔR and temperature were detected at the laser spot, when irradiated with the 785 nm laser (Fig. 2a, column 3), as at 1 mm away from the laser spot, when irradiated with the 532 nm laser (Fig. 2b, column 4), suggesting that the alteration induced by the 785 nm laser at the laser spot is thermally driven. We obtained similar results for realgar (Fig. S3†) and red lead when irradiating with 785 nm laser, suggesting a thermally dominated effect on all three pigments. The results obtained from irradiation with 785 nm and 1064 nm lasers have no signifi-

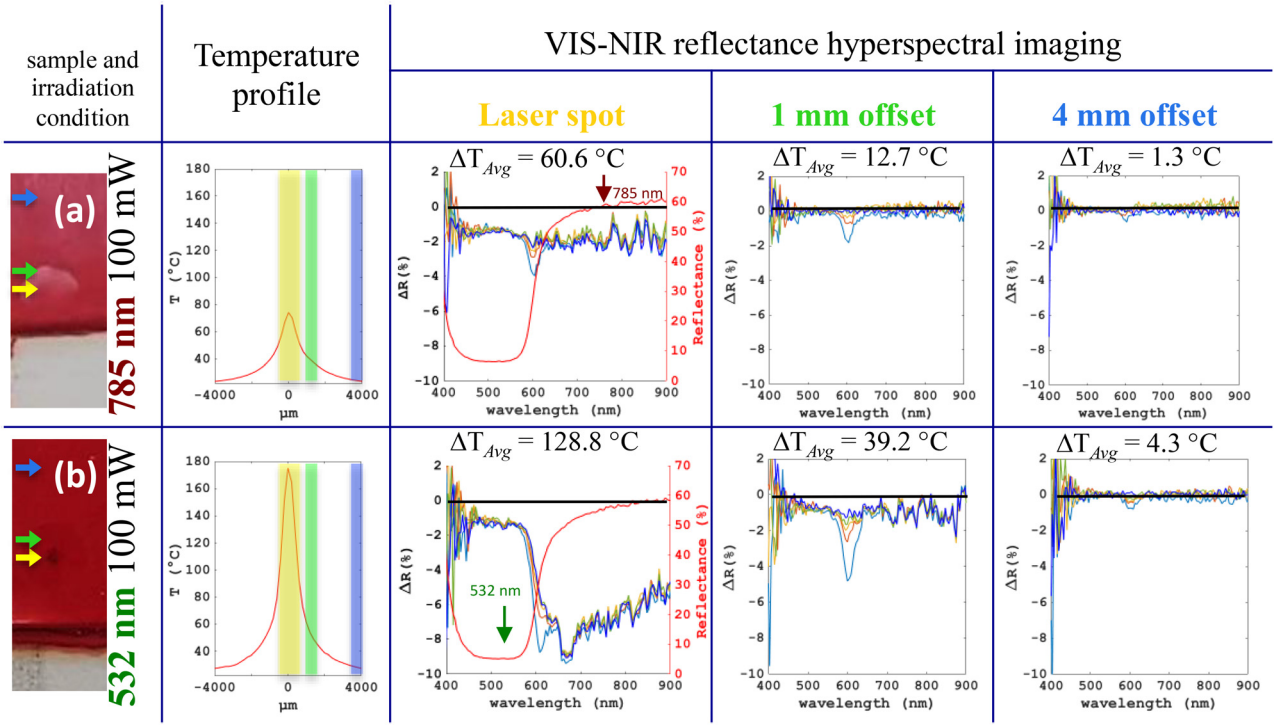

Fig. 2 Laser induced alteration dominated by thermal effects: vermilion oil paint mock-up irradiated at 100 mW with a spot size of 900 µm for 10 s with (a) 785 nm laser, and (b) 532 nm laser. Column 1: images of the sample around the irradiated areas (the yellow arrow indicates the position of the laser spot, green arrow is 1 mm offset and blue arrow is 4 mm offset from the laser spot); column 2: temperature profile just before turning off the laser (yellow, green and blue bands indicate the position of the laser spot, 1 mm and 4 mm offset from the laser spot); column 3: evolution of ΔR difference spectra measured with the HSI post irradiation at different times compared with pre-irradiation (1 s post irradiation shown in light blue, 5 s orange, 10 s yellow, 60 s green, 300 s dark blue) at the laser spot, and reflectance spectrum of the mock-up prior to irradiation (red curve) is also shown. Column 4: evolution of ΔR spectra 1 mm away from the centre of the laser spot; column 5: 4 mm away from the laser spot. The average temperature change (ΔT_{Avg}) is indicated in each case.

cant differences in terms of changes in reflectance, Raman spectra and surface temperature for all three pigments.

Further information can be extracted by comparing the hyperspectral cube and the thermal data cube in time and spatial extent as shown in Fig. 3. The time evolution of ΔR at 600 nm (Fig. 3a) gradually tends to a plateau as the temperature approaches room temperature. As ΔR at all wavelengths plateaus at a non-zero value (−2%) within the laser spot, there is an additional permanent change to the reversible change (Fig. 2a). Fig. 3B shows the intensity profile of the beam, the ΔT profile, and the reversible ΔR profile across the laser spot and its surrounding. Within the laser spot, the temperature and reversible ΔR profiles show a similar spatial trend; outside of the laser spot, the reversible ΔR profile show a deviation from the ΔT spatial trend, with a more gradual decrease in ΔR from the laser spot and an abrupt decrease occurring when the edge of the substrate was reached (Fig. 3b). The Ultra high resolution OCT was used to image the damaged area to obtain the RMS surface roughness map, showing a reduction in surface roughness, which is double the diameter of the laser spot (Fig. 3c).

It is important to note that permanent damage detectable by reflectance changes correlated with significant temperature rise (Fig. 2), are visible by eye but not by any Raman spectral changes (Fig. S4†). Moreover, no amorphization or phase transition was found when analysing thin sections obtained from the two irradiated spots with SR µ-XRPD mapping. Spectral reflectance monitoring allows a much more sensitive detection of permanent surface changes compared to Raman and even SR µ-XRPD. A decrease of the net peak counts of the main Raman bands of vermilion were detected only when irradiating with 532 nm at a much higher laser intensity, achieved by reducing the spot size from 900 to 180 µm while keeping the laser power and exposure time fixed (Fig. S5†). In this case a more severe darkening was observed (Fig. 4a). Vermilion darkening has been reported both as a natural degradation occurring in paintings[39–42] and induced by laser irradiation.[14] The mechanisms and the compounds that impart this darkening are still of open debate and due to the difficulty in identifying the degradation products and the highly superficial nature of the degradation. The laser-induced darkening has mainly been attributed to the formation of the black metacinnabar (β-HgS).[42,43] In the field of laser processing, a recent method has been proposed to produce the beta phase from the alpha phase using a pulsed 1064 nm laser.[44] Other recent studies explain the darkening as also due to a progressive amorphization of the alpha phase and possible defected alpha phase due

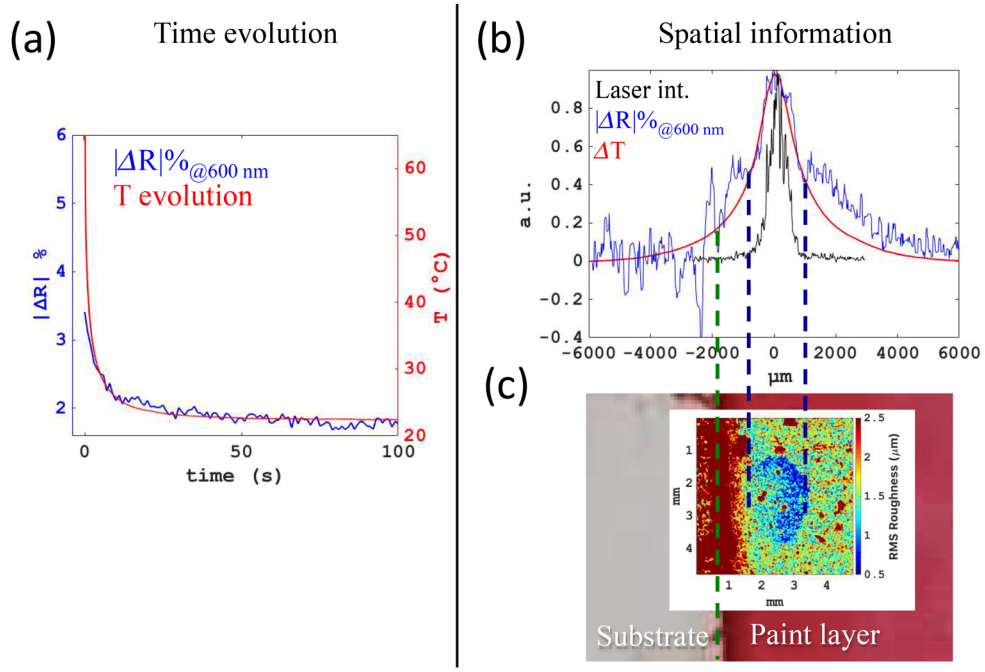

Fig. 3 Time and spatial evolution of the alteration. The same irradiation test of Fig. 2(a) on vermilion mock-up with 785 nm: (a) the time evolution of the reversible ΔR at 600 nm (blue curve) and the temperature evolution (red curve); (b) the spatial profile of the change in temperature ΔT (red), the reversible ΔR at 600 nm (blue) and the laser intensity (black). The spatial resolution of thermal camera (T), HSI (ΔR) and measurement of laser beam profile are 200 μm, 15 μm and 4.4 μm respectively. The curves are normalized to the peak value. (c) The RMS surface roughness map obtained within a 50 μm window from the ultra-high resolution OCT cube. The dark blue dashed lines define the edge of the damage. The green dashed line delineates the edge between the paint layer and the substrate.

to sulfur deficiencies.[45,46] In our experiments, the SR μ-XRPD mapping of the thin section of the most severely darkened area (Fig. 4) revealed a reduction of the peaks ascribed to cinnabar on the surface and a slight asymmetric broadening of some cinnabar peaks. Extracting diffraction patterns from the cross-sectional layers (the top 5 μm, the sub-surface layer 5–10 μm in depth, and the bulk of the paint layer 10 to 20 μm in depth) (Fig. 4d), it is possible to observe also a weak peak appearing as a shoulder at a smaller angle next to the most intense peak of cinnabar, which can indicate the presence of metacinnabar (the 200 Bragg peak, 9008849 COD inorganics[38]). All these features could indicate the possible formation of very small particles of metacinnabar produced on the top few microns of the irradiated area, as shown by the Red-Green false colour combination map in Fig. 4c.

Thus, a surface darkening detected by HSI was produced on the vermilion oil mock-up at 100 mW both with a spot size of 900 μm (Fig. 2b) and with a spot of 180 μm (Fig. 4). However, only in the latter case, where the intensity is 20 times higher, a subtle crystal transformation in μ-XRPD was detected and a reduction of the main Raman peaks of vermilion was observed. The darker surface of the high intensity test absorbs many more incident photons, leaving significantly less photons for Raman scattering of the unaltered vermilion below the surface, and hence a reduced Raman signal of vermilion.

To assess the effect of the binding medium, the irradiation test at 100 mW using the 532 nm laser was replicated on the vermilion powder. In this case, the temperature rose to 210 °C, a more severe darkening occurred, and the main Raman peak of vermilion reduced in intensity (Fig. S6†). The different behavior of the pigment powder and the oil paint of the same pigment may suggest a better heat dissipation of the oil binder, which was suggested also in another study.[24] This comparison highlights how important it is to study the laser interaction of the pigments in the specific binding medium of interest, to avoid misleading conclusions on the potential damage.

Intensity is known to be one of the key parameters that increase damage risk, but a prolonged exposure (increase of fluence or total energy per unit area irradiated) may also have its impact that needs to be investigated. At a laser intensity where a short irradiation time (10 s) did not cause permanent damage with the 785 nm laser, the prolonged exposure (up to 450 s) did not cause further damage for any of the three pigments either (see Fig. S7† for an example on red lead). In these cases, a temperature plateau is reached after a few seconds of irradiation. This data suggests that for safe operation at 785 nm where thermal effects dominate with these pigments, it is preferable to operate at low laser intensity with increased exposure time to obtain the same SNR Raman signal.

3.2. Contribution of photochemical effects

Fig. 5 shows the results of a realgar oil paint mock-up irradiated with the 532 nm laser, where different types and extents

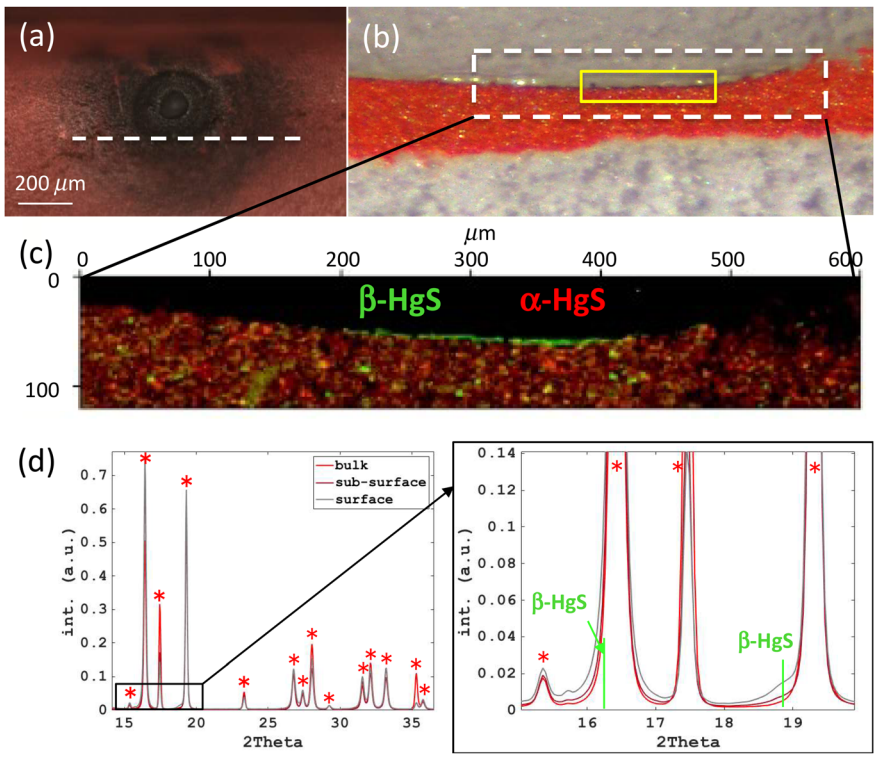

Fig. 4 Laser induced crystal structural change of vermilion. Results of vermilion oil mock-up irradiation with the 532 nm laser for 10 s at 100 mW and a spot size of 180 μm. (a) The optical microscope image of the darkened surface; (b) the thin section of 10 μm obtained from the sample (yellow area corresponds to laser spot, dashed white rectangle is the analysed area); (c) the Red/Green composite SR μ-XRPD map of respectively α-HgS/β-HgS; (d) the average XRD patterns from the first 5 μm of the surface (grey curve), from sub-surface 5 to 10 μm (dark red curve) and from the bulk 10–20 μm (red curve), with * indicating the Bragg peaks of α-HgS and vertical green lines indicating the β-HgS Bragg peaks.

of damage occurred depending on the intensity and exposure time. The high-power test (100 mW) induced a permanent increase of percentage reflectance around 540 nm (up to 7%) and a significant temperature rise to 128 °C (Fig. 5a). The heat dissipation away from the irradiated spot resulted in the detection of only a reversible ΔR at around 565 nm, which gradually disappeared away from the laser spot. With a reduced power of 2.8 mW, the temperature rise was minimal (2–3 °C) and only the permanent damage at around 540 nm was present though considerably reduced within the laser spot (Fig. 5b). In comparison, a similar temperature rise of 2–3 °C was detected 4 mm away from the laser spot in the high-power test (Fig. 5a), where only the reversible ΔR at 565 nm was detected, indicating that a purely thermal contribution of 2–3 °C without photon irradiation does not cause permanent damage. Therefore, the permanent damage seen in the low-power test at the laser spot is likely to be of non-thermal origin.

The effect of a prolonged exposure time was tested at low power (2.8 mW) irradiating for 450 s (Fig. 5c). The temperature rise (2–3 °C) is comparable to the 10 s exposure but a permanent reflectance change of −11% (*cf.* 7% for 10 s) appeared at a different wavelength of 580 nm (*cf.* 540 nm for 10 s). The damage is visible by eye as an orange spot with dimensions comparable to the laser spot size (900 μm). In this non-thermal dominated effect, the prolonged exposure resulted in increased damage, in contrast to the thermally dominated case observed with 785 nm laser.

The capability of hyperspectral imaging to distinguish the spatial extent of different reflectance changes within the same dataset is highlighted in Fig. 6. We can see that under high power (100 mW) at 532 nm, the permanent reflectance change ΔR at 540 nm appeared only within the laser spot where photons were incident on the sample (Fig. 6a), while the reversible ΔR at 565 nm steadily decreased away from the laser spot and showed a similar trend to the temperature profile (Fig. 6b). This data suggests the presence of two competing effects, thermal and non-thermal, when irradiating the realgar paint mock-up with 532 nm laser at high intensity.

It is well known that realgar is particularly susceptible when irradiated at around 500–670 nm as a photochemical transformation to pararealgar occurs.[47]

Several studies show that the process undergoes several intermediate steps related to a progressive, randomly distributed change of the As_4S_4 into As_4S_5 cages,[48–50] also called χ phase in early literature.[47] In our experiments, the possible crystal structure change of realgar to pararealgar induced by 532 nm laser can be seen in the changes observed in the Raman spectra collected before and after the irradiation (Table 1 and Fig. S8†). However, no peaks ascribed to pararealgar were detected and only a decrease of intensity of the main

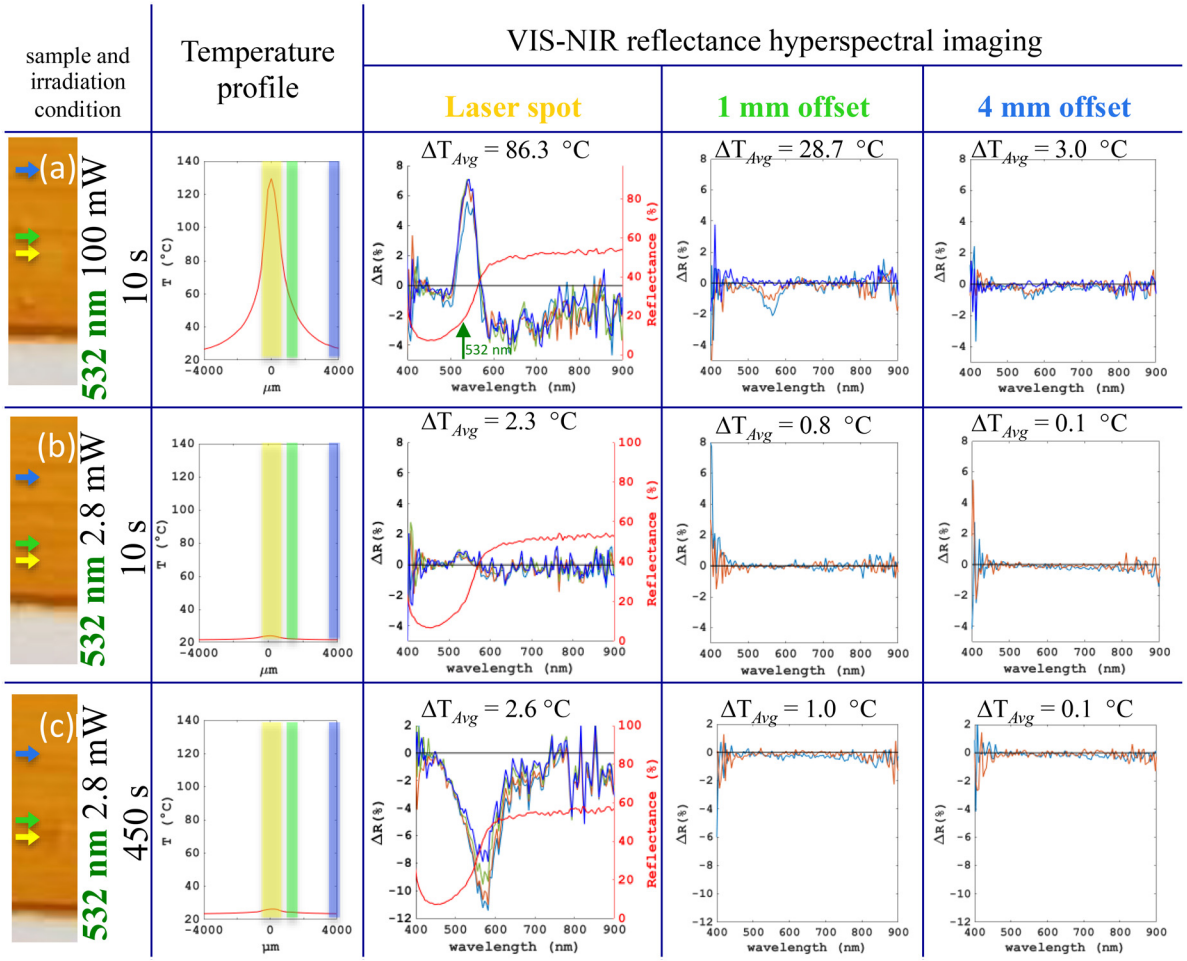

Fig. 5 The thermal and photochemical effects on realgar paint mock-up irradiated with 532 nm laser with a spot size of 900 μm (a) at 100 mW for 10 s; (b) at 2.8 mW for 10 s; (c) at 2.8 mW for 450 s. Column 1: images of the irradiated areas (the yellow arrow indicates the position of the laser spot, green arrow is 1 mm offset and blue arrow is 4 mm offset from the laser spot); column 2: temperature profile just before turning off the laser (yellow, green and blue bands indicate the position centered at the laser spot, 1 mm and 4 mm offset from the laser spot); column 3: ΔR difference reflectance spectra (1 s light blue, 5 s orange, 10 s yellow, 60 s green, 300 s dark blue) at the position of the laser irradiation, and the reflectance spectrum of the mock-up prior to irradiation (red curve). Column 4: evolution of ΔR spectra 1 mm away from the centre of the laser spot; column 5: 4 mm away from the laser spot. The average temperature change (ΔT_{Avg}) is indicated in each case.

realgar peaks after irradiation was observed for the high-power short-exposure test and the low-power long-exposure test (Table 1). To further assess the possible formation of pararealgar, a thin section of these two tests subjected to the same total energy of radiation, high-power short-exposure and the low-power long-exposure, were analysed with SR μ-XRPD mapping. Extracting diffraction patterns from every 5 μm going from surface to bulk shows that in the irradiated area of the high-power test (Fig. 6c and d), a 10–15 μm layer of pararealgar was produced followed by a thin intermediate layer with a small quantity of the χ phase with pararealgar before reaching the unreacted bulk. Peaks ascribed to the presence of a discontinuous thin layer (*ca.* 5 μm) of pararealgar with a higher amount of the intermediate χ phase are already present due to the age of the mock-up (15 years old) as shown in an area outside the laser spot (Fig. 6d, diffractogram on the right). A similar composition to the pristine paint is detected in the SR μ-XRPD map of the low-power long-exposure test (Fig. S9†), suggesting that this type of irradiation did not clearly produce a pararealgar layer. It is known that for some pigments, and in specific intensity range, reciprocity can fail, meaning that the amount of degradation depends not only on the total energy that the sample is exposed to, but also the light intensity. It has been found that in the case of broadband light-induced alteration of realgar, reciprocity does not hold even within one order of magnitude in intensity.[51] In our case, reciprocity do not hold over one order of magnitude in power and the failure of the reciprocity principle may be attributed to a high contribution of thermal effects at high power and dominance of non-thermal effects (photochemical) at low power.

3.3. Identification of damage prediction marker

The interaction between the 785 nm laser and the investigated pigments has shown a predominant thermal effect. In this

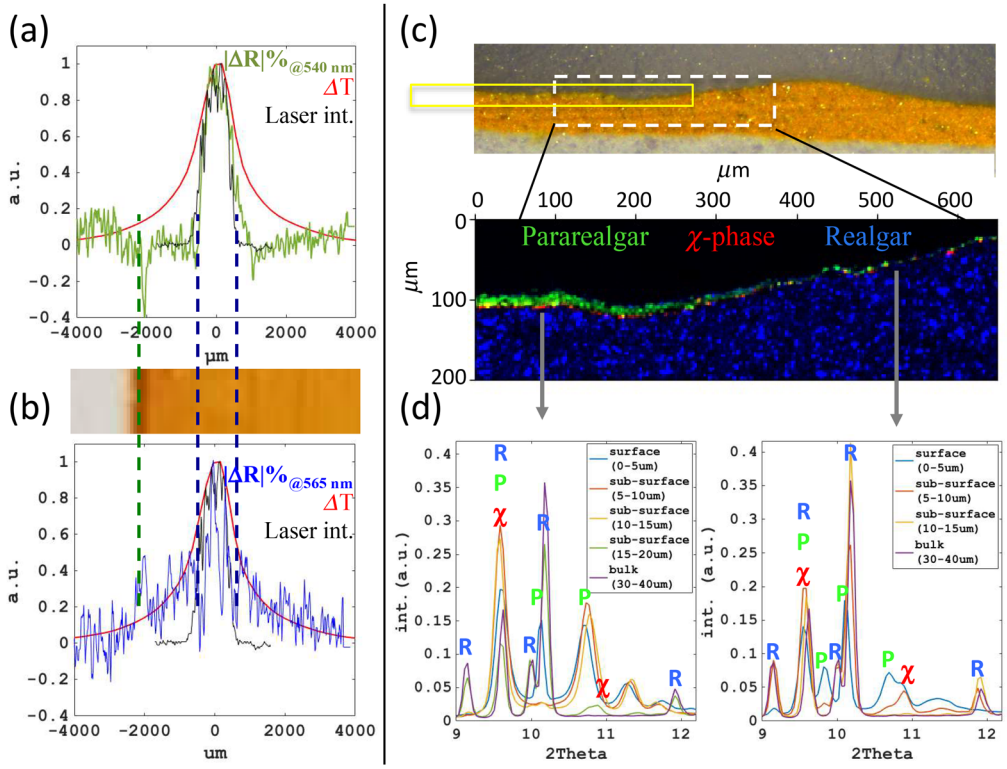

Fig. 6 Photochemical and thermal contributions in the alteration of realgar paint sample irradiated for 10 s with 532 nm laser at 100 mW and spot size of 900 μm. (a) spatial variation of the permanent reflectance change ΔR at 540 nm compared with the temperature and the laser intensity profile; (b) the reversible reflectance change ΔR at 565 nm; (c) the thin section (10 μm) of the sample (yellow area corresponds to laser spot, dashed white rectangle is the analysed area) and the red/green/blue composite SR μ-XRPD map of χ phase/pararealgar/realgar respectively; (d) the averaged diffraction patterns from each 5 μm in depth of the thin section from the area irradiated by the laser and from an area out of the laser spot. Realgar (R), pararealgar (P) and the χ phase (χ) were identified.

Table 1 Raman monitoring of realgar paint mock-up irradiated with 532 nm laser

532 nm on realgar[a]	Δ Raman shift[b] (cm^{-1})	Δ net peak counts[c]
2.8 mW, 10 s	−0.3 ± 0.8	−12.6 ± 13.5
2.8 mW, 450 s	−0.7 ± 0.8	−40.7 ± 11.1
100 mW, 10 s	−0.3 ± 1.0	−47.3 ± 12.6

[a] Irradiation of the paint mock-up with a spot size of 900 μm. [b] Raman spectral difference in peak position between pre and post irradiation of the main characteristic peak of realgar (354 cm^{-1}). Raman spectra collected with 785 nm. [c] Raman spectral difference in neat peak counts between pre and post irradiation of the main characteristic peak of realgar (354 cm^{-1}).

regime, by increasing the laser power (Fig. 7) we observed that the first alteration detected is a reversible spectral reflectance change ΔR (Fig. 7b), and permanent damage eventually appeared only when the laser power was increased further (Fig. 7c and d). The occurrence of a reversible ΔR prior to permanent damage has been observed in all three pigments irradiated with the 785 nm laser. This data suggests that reversible ΔR can be identified as a damage prediction marker. In the predominantly photochemical effect that occurred in the case of realgar with 532 nm laser at low powers, a prediction marker was not detected. Nevertheless, the very high sensitivity of the HSI allows detecting even subtle changes (Fig. 5b) not detected by Raman or SR μ-XRPD, nor by the naked eye.

3.4. Safety threshold

The identification of LIDT is generally performed by varying laser power for a given setup and is expressed in terms of the minimum laser intensity at which damage is observed. When dealing with Raman spectroscopy for sensitive materials, such as heritage objects, a balance must be struck between efficiency in collecting Raman photons and safe limits to avoid damage. Thanks to the reversible reflectance changes (ΔR) appearing prior to thermally dominated permanent damage, we can use this prediction marker to objectively define the safety threshold.

As shown in the earlier sections, apart from intensity, the duration of irradiation can contribute to the damage. Only recently, it was found that the laser spot size has an effect as well, independent from intensity.[14,17] It is quite common to refer to micro-Raman as a riskier technique compared to portable Raman, due to the smaller spot size exploited in micro-Raman (from hundreds of μm for portable devices to just few μm for micro-Raman) that increases considerably the intensity for a given laser power.[52] This consideration assumes that the

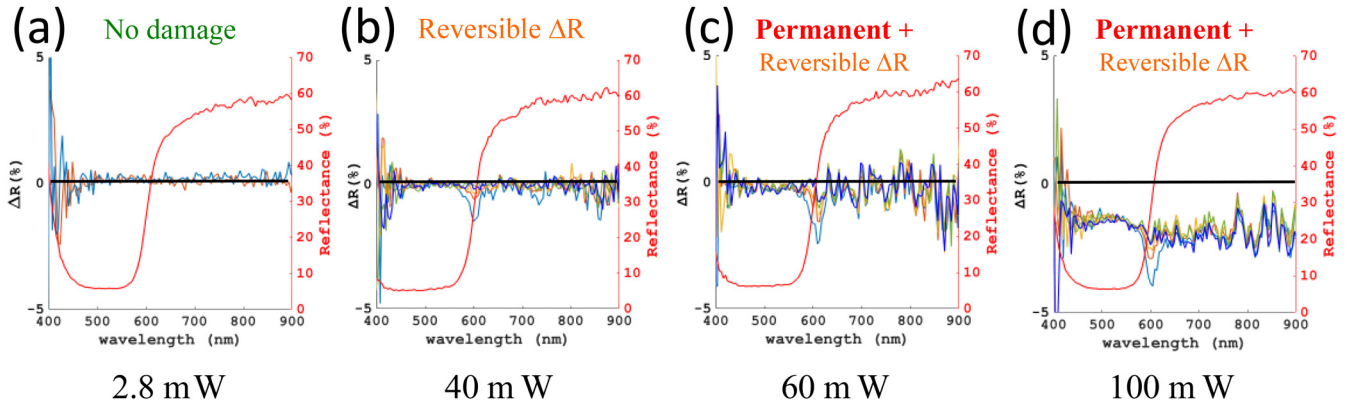

Fig. 7 The reversible ΔR as prediction marker: the ΔR VIS-NIR changes (1 s light blue, 5 s orange, 10 s yellow, 60 s green, 300 s dark blue) and initial reflectance spectrum (in red) of vermilion oil mock-up irradiated with the 785 nm laser with a laser spot of 900 μm for 10 s at increasing laser power: (a) 2.8 mW, (b) 40 mW; (c) 60 mW; (d) 100 mW.

intensity damage threshold is independent of other laser parameters. However, by plotting safety threshold (*i.e.*, laser intensity when only reversible ΔR is observed) and the LIDT (*i.e.*, at the threshold of permanent ΔR appearing) at fixed exposure time for various spot sizes between 40 μm and 900 μm (Fig. 8a), it is clear that spot size has a considerable effect. If we compare spot sizes of 40 μm and 900 μm, the safety threshold in laser intensity is at least 90 times lower for the larger spot size than that for the smaller one, while in contrast, the safety threshold in laser energy (or power at the same irradiation time) is around 5 times higher for the larger spot size (Fig. 8b). This means that in this example, under safe operation, the larger spot size can be up to 5 times more time efficient in collecting Raman photons than the smaller spot size, assuming the total laser energy incident at the sample is proportional to the Raman photons generated. Delivering the same 532 nm high laser intensity (20.8 W cm^{-2}) with different spot sizes on vermilion mock-up, shows that the bigger the spot the more severe the damage and the higher the surface temperature (Fig. 8c). This effect can clearly be the result of better heat dissipation in smaller volumes than those of larger spot and volume as already hypothesized in previous works.[14,17] However, it is interesting to note that this trend is observed not only on vermilion oil paint with a high intensity laser, but also on realgar at a low intensity (0.5 W cm^{-2}) where there is no significant temperature rise detected (Fig. 8d). In summary, for a comprehensive assessment of damage and safety threshold we need to consider not only intensity but instead the 3 experimental parameters: power, duration of irradiation, and spot size in combination.

4. Discussion

The identification of LIDT on mock-ups is intrinsically an unreliable method owing to the highly heterogeneous nature of artists' materials. Research effort should focus on developing monitoring strategies to prevent damage while measuring with laser-based techniques. The inspection technique used to detect damage must also measure directly material alterations and be sensitive to low level alterations to mitigate damage. In this work, we have demonstrated the effectiveness of VIS-NIR HSI in detecting a broad variety of laser-induced alterations on representative artist materials, providing information both on the spatial extent and the evolution over time of the possible damage. We have shown that the very high sensitivity of reflectance spectroscopy allowed us to detect subtle changes not detectable visually, even under a microscope. The minimum laser intensity at which we can see permanent alteration with HSI is at least a factor 20 lower than that detectable by Raman spectroscopy (Fig. 2b and 4). The HSI monitoring over time enabled us to identify a transient change in reflectance that appears prior to permanent damage (Fig. 7), when the effect is thermally driven. Owing to the intrinsic sensitivity of reflectance spectroscopy to laser induced alterations, damage can be effectively mitigated. Moreover, in the case of photothermal damage, this prediction marker can be used to prevent damage. Hence the method can objectively define the safety threshold and is suitable for safe Raman measurements directly on real historical materials without the need to perform unreliable preliminary tests on mock-ups to define LIDT. Monitoring of radiation damage during Raman measurements *in situ* may be more convenient with a simpler system using reflectance spectroscopy, similar to the setup in our previous work.[17]

A deeper understanding of the laser-material interaction allows the design of a better damage mitigation strategy when measuring real artists' materials. Thanks to the lateral resolution and field of view of the HSI, it is possible to detect alterations not only in areas directly irradiated with photons but also in regions away from that, where the dissipated heat from the laser spot has an effect. The multi-modal set-up with time and spatially resolved thermal and spectral reflectance monitoring allowed the distinction between spectral changes associated with photochemical and thermal effects (Fig. 6a and b). The heat accumulation induced by increased laser intensity is

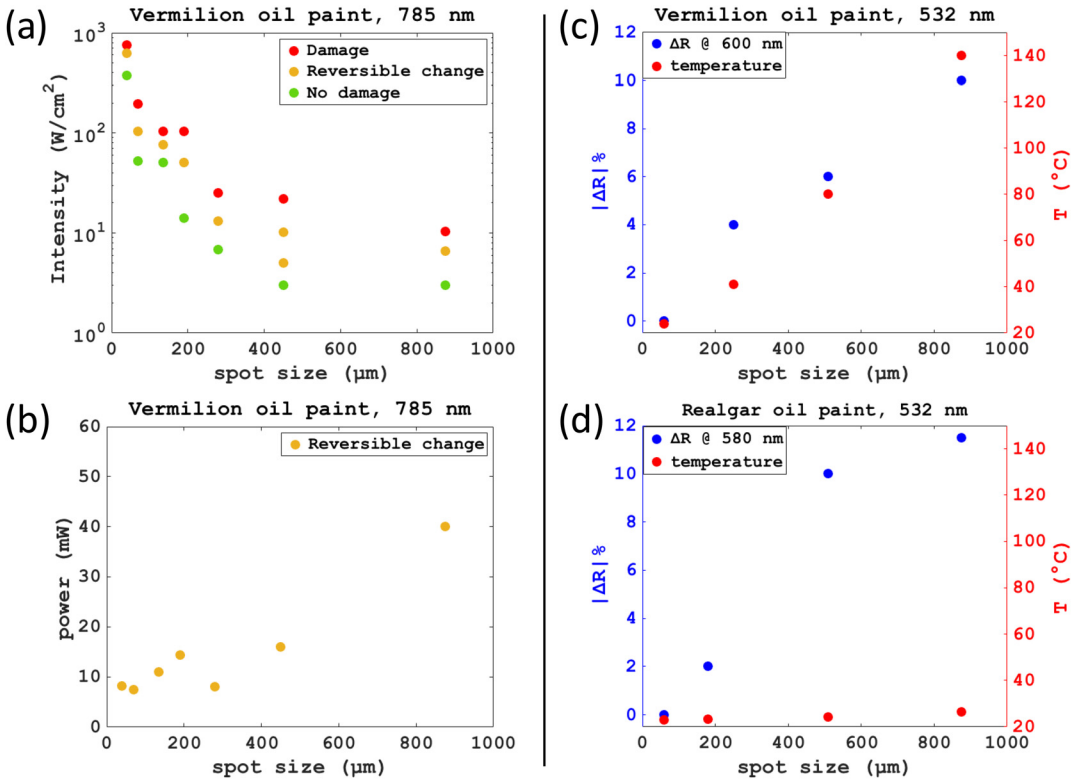

Fig. 8 The safety threshold and the effect of spot size. (a) Intensity damage threshold (red, corresponding to permanent reflectance changes, ΔR), safety threshold (orange, corresponding to only reversible reflectance changes) and no alteration (green, no reflectance changes) for different spot sizes of 785 nm laser irradiation for 10 s on vermilion oil paint mock-up and in (b) the corresponding incident power at each spot size for safe operation. (c) The maximum absolute spectral reflectance changes $|\Delta R|$ after 1 s of 532 nm laser irradiation with different spot sizes at the same intensity of 20 W cm^{-2} for 10 s for vermilion mock-up ($|\Delta R|$ at 600 nm) and (d) at 0.5 W cm^{-2} for 450 s for realgar mock-up ($|\Delta R|$ at 580 nm).

well known, but here we demonstrated that it is necessary to consider the combined effect of the 3 parameters, power, spot size, and exposure time, to define safety thresholds. Through this, some not so commonly known effects were found. The laser induced damage threshold in intensity considerably decreases when using a larger spot size, that is, it is less safe to use a larger spot size for the same laser intensity. Prolonging the irradiation time does not necessarily increase the extent of damage. While prolonged exposure caused a significant increase in the extent of damage in a case where photochemical effect dominated (Fig. 5b and c), it did not increase the extent of damage in another case where the thermal effect dominated (Fig. S5†). We aim to explore further the spot size effect on the damage threshold. In particular, to identify the optimum combination of power, spot size and exposure time for the highest SNR Raman signal within safe operation limits.

The three selected pigments present similar absorption and scattering properties in the VIS-NIR regime (absorbing at 532 nm and highly scattering at 785 and 1064 nm) but demonstrated different responses to laser irradiation. Red lead paint mock-up proved to be very resistant to the three lasers (532, 785 and 1064 nm) investigated, with no permanent damage detected in the survey (maximum laser power 100 mW). The vermilion oil paint mock-up appeared to be damaged mainly by thermal effects, with 532 nm laser causing the highest temperature rise. The vermilion oil paint was heated up less than the vermilion powder and resulted in less damage under the same irradiation conditions. In the most severely darkened case, a very thin layer of black *meta*-cinnabar was formed (Fig. 4). To a higher or lower extent, a superficial layer of para-realgar and intermediate phases were produced when realgar was irradiated with 532 nm laser (Fig. 6c, d and Fig. S6†). With the predominant thermal effect induced by the 785 nm and 1064 nm lasers, realgar exhibited a relative stability to temperature rises. Overall, when irradiating with 785 nm and 1064 nm laser, the resultant temperature rise is highest on the vermilion mock-up, followed by realgar and then red lead (Fig. 2a and Fig. S3, S5† respectively). The surface temperature rises due to both absorption and scattering, and the kinetics of cooling are mainly related to the heat capacity of the irradiated materials. The lowest reported heat capacity is the one of vermilion (48.4 J K^{-1} mol^{-1}), followed by realgar (82.9 J K^{-1} mol^{-1}) and then red lead with the highest heat capacity (130 J K^{-1} mol^{-1}).[53,54] These results indicate that both light stability and thermal stability are important in determining how sensitive a pigment is to laser irradiation. Experiments are in progress to further assess laser induced reflectance changes on other pigments and in mixtures.

5. Conclusions

The multimodal imaging set-up is valuable for understanding and studying different damage mechanisms and contributes to the development of a safe analytical protocol for Raman spectroscopy on paintings. Owing to the extremely high sensitivity of VIS-NIR reflectance spectroscopy in detecting even subtle changes, it is an effective monitoring technique to be used in tandem during laser-based analyses. It could also be applied to the monitoring of other types of radiation, such as X-ray, for safe analysis of paintings. Furthermore, its application could also be extended to other fields, such as laser processing where a high control of intentional laser induced modifications are required.

Author contributions

Conceptualization: A. S., H. L., C. R. Methodology: H. L., A. S., C. S. C., C. R. Software: A. H., P. A., Y. L. Resources: A. H., C. S. C. Investigation: A. S., C. S. C., Y. L. Validation: A. S., H. L. Visualization: A. S., H. L., P. A., Y. L. Supervision: H. L., C. R., C. M. Writing – original draft: A. S. Writing – review & editing: H. L. and all. Funding: H. L., C. R., C. M.

Data availability

All data are available in the main text or the ESI.† Raw data can be made available upon reasonable request. The μ-XRD data are available in the ESRF repository.[34]

Conflicts of interest

The authors declare that they have no competing interests.

Acknowledgements

This work is partially funded by the IPERION HS project which has received funding from the European Union's Horizon 2020 research and innovation programme under Grant Agreement n. 871034. Funding from the UK Arts and Humanities Research Council (AHRC AH/V012460/1) is gratefully acknowledged. We acknowledge the European Synchrotron Radiation Facility for provision of synchrotron radiation facilities (proposals HG-172 Structural analysis of historical materials) and we would like to thank Dr Alexey Melnikov and Jiliang Liu for assistance in using beamline ID13 (proposal HG-172, pilot of a BAG project supported by the European Union's Horizon 2020 research and innovation programme under grant agreement No 870313, Streamline). A. S. acknowledge Nottingham Trent University for her PhD studentship funding.

References

1 B. Brunetti, C. Miliani, F. Rosi, B. Doherty, L. Monico, A. Romani and A. Sgamellotti, *Top. Curr. Chem.*, 2016, **374**, 10.
2 L. Bertrand, S. Schöeder, D. Anglos, M. B. H. Breese, K. Janssens, M. Moini and A. Simon, *TrAC, Trends Anal. Chem.*, 2015, **66**, 128–145.
3 IPERION HS, Integrating Platform for the European Research Infrastructure on Heritage Science, H2020-INFRAIA-2019-1, under GA 871034. **https://www.iperionhs.eu**.
4 D. Bersani and J. M. Madariaga, *J. Raman Spectrosc.*, 2012, **43**, 1523–1528.
5 G. Marucci, A. Beeby, A. W. Parker and C. E. Nicholson, *Anal. Methods*, 2018, **10**, 1219–1236.
6 Y. Li, C. S. Cheung, S. Kogou, A. Hogg, H. Liang and S. Evans, in *ICOM-CC 19th Triennial Conference Preprints*, Beijing, 17–21 May 2021, ed. J. Bridgland, International Council of Museums, Paris. **https://www.icom-cc-publications-online.org/4478/Standoff-laser-spectroscopy-for-wall-paintings-monuments-and-architectural-interiors**.
7 P. Vandenabeele and A. Rousaki, *Anal. Chem.*, 2021, **93**, 15390–15400.
8 L. Burgio, R. J. H. Clark and S. Firth, *Analyst*, 1001, **126**, 222–227.
9 G. Moretti and C. Gervais, *J. Raman Spectrosc.*, 2018, **49**, 1198–1204.
10 G. D. Smith, L. Burgio, S. Firth and R. J. H. Clark, *Anal. Chim. Acta*, 2001, **440**, 185–188.
11 ISO 21254-1:2011(en) - International Organization for Standardization. **https://www.iso.org/obp/ui/#iso:std:iso:21254:-1:ed-1:v1:en** (Accessed on 24 October 2022).
12 J. L. Ruvalcaba-Sil, E. Casanova-González, N. A. Pérez-Castellanos and M. A. García-Bucio, *J. Raman Spectrosc.*, 2013, **44**, 1711–1717.
13 N. C. Sherrer, in the 6th international Congress on the Application of Raman Spectroscopy in Art and Archaeology, Parma, Italy, Book of abstracts, 203–204 (2011).
14 A. Philippidis, A. Mikallou and D. Anglos, *Eur. Phys. J. Plus*, 2021, **136**, 1194.
15 A. De Santis, E. Mattei and C. Pelosi, *J. Raman Spectrosc.*, 2007, **38**, 1368–1378.
16 M. Oujja, P. Pouli, C. Domingo, C. Fotakis and M. Castillejo, *Appl. Spectrosc.*, 2010, **64**, 528–536.
17 Y. Li, A. Suzuki, C. S. Cheung, Y. Gu, S. Kogou and H. Liang, *Eur. Phys. J. Plus*, 2022, **137**, 1102.
18 A. Suzuki, Y. Li, Y. Gu, C. S. Cheung, C. Riminesi and H. Liang, in Optics for Arts, Architecture, and Archaeology VIII (SPIE, 2021, Munich), Proc. SPIE vol. 11784, p. 117840N. **https://www.spiedigitallibrary.org/conference-proceedings-of-spie/11784/2593925/Investigation-of-laser-induced-damage-to-historical-paint-during-Raman/10.1117/12.2593925.short**.
19 K. S. K. Varadwaj, M. K. Panigrahi and J. Ghose, *J. Solid State Chem.*, 2004, **177**, 4286–4292.

20 E. Mattei, G. de Vivo, A. De Santis, C. Gaetani, C. Pelosi and U. Santamaria, *J. Raman Spectrosc.*, 2008, **39**, 302–306.
21 M. Hanesch, *Geophys. J. Int.*, 2009, **177**, 941–948.
22 D. Ciofini, J. Agresti, A. A. Mencaglia, S. Siano and I. Osticioli, *Sens. Actuators, B*, 2020, **325**, 128958.
23 A. A. Mencaglia, I. Osticioli and S. Siano, *Measurement*, 2018, **118**, 372–378.
24 C. Calvagna, A. A. Mencaglia, I. Osticioli, D. Ciofini and S. Siano, *Sensors*, 2022, **22**, 2680.
25 H. Liang, *Appl. Phys. A*, 2012, **106**, 309–323.
26 A. Macchia, L. Campanella, D. Gazzoli, E. Gravagna, A. Maras, S. Nunziante, M. Rocchia and G. Roscioli, *Procedia Chem.*, 2013, **8**, 185–193.
27 A. Čiuladienė, A. Luckutė, J. Kiuberis and A. Kareiva, *Chemija*, 2018, **29**, 243–256.
28 P. Ballirano and A. Maras, *Eur. J. Mineral.*, 2006, **18**, 589–599.
29 D. Chiriu, M. Pala, F. A. Pisu, G. Cappellini, P. C. Ricci and C. M. Carbonaro, *Dyes Pigm.*, 2021, **184**, 108866.
30 P. Ballirano, M. Botticelli and A. Maras, *Eur. J. Mineral.*, 2013, **25**, 957–965.
31 Y. Li, S. C. Cheung, S. Kogou, F. Liggins and H. Liang, *Opt. Express*, 2019, **27**, 31338–31347.
32 C. S. Cheung, M. Spring and H. Liang, *Opt. Express*, 2015, **23**, 10145–10157.
33 S. Lawman and H. Liang, *in*: *O3A*: *Optics for Arts, Architecture, and Archaeology II, SPIE*, 2009: pp. 151–162. DOI: **10.1117/12.827518**.
34 Historical Materials BAG access. Data DOI: **10.15151/ESRF-ES-931197247**, DOI: **10.15151/ESRF-ES-1171320945**.
35 M. Cotte, V. Gonzalez, F. Vanmeert, L. Monico, C. Dejoie, M. Burghammer, L. Huder, W. de Nolf, S. Fisher, I. Fazlic, C. Chauffeton, G. Wallez, N. Jiménez, F. Albert-Tortosa, N. Salvadó, E. Possenti, C. Colombo, M. Ghirardello, D. Comelli, E. Avranovich Clerici, R. Vivani, A. Romani, C. Costantino, K. Janssens, Y. Taniguchi, J. McCarthy, H. Reichert and J. Susini, *Molecules*, 2022, **27**, 1997.
36 J. Kieffer, V. Valls, N. Blanc and C. Hennig, *J. Synchrotron Radiat.*, 2020, **27**, 558–566.
37 V. A. Solé, E. Papillon, M. Cotte, P. Walter and J. Susini, *Spectrochim. Acta, Part B*, 2007, **62**, 63–68.
38 **https://www.crystallography.net/cod/**(Accessed on 20 August 2023).
39 M. Spring and R. Grout, *Natl. Gallery Tech. Bull.*, 2002, **23**, 50–61.
40 M. Cotte, J. Susini, N. Metrich, A. Moscato, C. Gratziu, A. Bertagnini and M. Pagano, *Anal. Chem.*, 2006, **78**, 7484–7492.
41 E. Gliozzo, *Archaeol. Anthropol. Sci.*, 2021, **13**, 210.
42 J. Yu, W. Warren and M. Fisher, *Sci. Adv.*, 2019, **5**, eaaw3136.
43 M. Oujja, M. Sanz, E. Rebollar, J. F. Marco, C. Domingo, P. Pouli, S. Kogou, C. Fotakis and M. Castillejo, *Spectrochim. Acta, Part A*, 2013, **102**, 7–14.
44 N. J. Mohammed and H. F. Dagher, *J. Mater. Sci.*, 2020, **17**, 11–16.
45 H. Béarat, A. Chizmeshya, R. Sharma, A. Barbet and M. Fuchs, *in the Third International Conference on Science and Technology in Archaeology and Conservation*, Jordan, 7 to 11 December 2004, pp. 53–70.
46 F. A. Pisu, M. Marceddu, P. C. Ricci, C. Melis, S. Porcu, C. M. Carbonaro and D. Chiriu, *J. Photochem. Photobiol., A*, 2023, **435**, 114291.
47 D. L. Douglass, C. Shing and G. Wang, *Am. Mineral.*, 1992, **77**, 1266–1274.
48 P. Bonazzi, L. Bindi, G. Pratesi and S. Menchetti, *Am. Mineral.*, 2006, **91**, 1323–1330.
49 A. Kyono, *J. Photochem. Photobiol., A*, 2007, **189**, 15–22.
50 E. Gliozzo and L. Burgio, *Archaeol. Anthropol. Sci.*, 2021, **14**, 4.
51 H. Liang, R. Lange, A. Lucian, P. Hyndes, J. H. Townsend and S. Hackney, in the ICOM Committee for Conservation 16th Triennial Meeting, Lisbon, Portugal 19–23 September 2011, **https://www.icom-cc-publications-online.org/1291/Development-of-portable-microfading-spectrometers-for-measurement-of-light-sensitivity-of-materials**.
52 O. N. Shebanova and P. Lazor, *J. Raman Spectrosc.*, 2003, **34**, 845–852.
53 P. Garnier, J. F. Berar and G. Calvarin, *Mater. Res. Bull.*, 1979, **14**, 1275–1279.
54 O. Madelung, *Semiconductors: Data Handbook*, Cleaver-Hume, 2004.